Research Article

Comparison of Dynamic Responses of Parallel-Placed Adjacent High-Rise Buildings under Wind and Earthquake Excitations

Huaxiao Wu (ID),[1] **Qinhua Wang** (ID),[2] **Nayan Deep Tiwari** (ID),[1] **and Dario De Domenico** (ID)[3]

[1]*Department of Civil and Environmental Engineering, Shantou University, Shantou 515063, China*
[2]*School of Civil Engineering and Architecture, Southwest University of Science and Technology, Mianyang 621010, China*
[3]*Department of Engineering, University of Messina, Messina 98166, Italy*

Correspondence should be addressed to Qinhua Wang; qinhuawang@stu.edu.cn

Two parallel-placed adjacent high-rise buildings are often linked to each other through passive control devices for vibration mitigation purposes. The mitigation efficiency of these control devices mainly depends on the characteristics of relative dynamic responses, namely, opposite-sign and same-sign responses of the two buildings. The present research first identifies an opposite-sign response factor to estimate the time ratio of opposite-sign responses. Subsequently, a structure comprising two adjacent high-rise buildings (with different natural frequency ratios) subjected to both wind and earthquake excitations is analyzed. Wind-induced responses are evaluated based on wind loads obtained from wind tunnel tests, while earthquake responses are determined through a suite of 44 natural ground-motion records. The results indicate that opposite-sign factors of the displacement, velocity, and acceleration responses under wind loads, especially at across-wind direction, are larger than those under earthquake excitations, and opposite-sign response factors under wind loads are insensitive to variation of the natural frequency ratio of the two adjacent buildings compared with those under earthquake excitations. The conclusions of this research may be helpful for wind-resistant and antiseismic design of parallel-placed adjacent high-rise buildings.

1. Introduction

With the rapid development of metropolitan cities over the years, high-rise buildings are often constructed in close proximately to each other [1]. Some notable examples of such attractive building systems include the Petronas Twin Towers in Kuala Lumpur, the Marina Bay Sands Hotel, American Coopers in New York, and many more. These slender parallel-placed adjacent high-rise buildings are sensitive to dynamic excitations [2–4]. When these buildings are located in regions prone to hurricanes and earthquakes simultaneously, they may suffer from significant damage in their uncontrolled configurations. Hence, various passive control devices may be installed on these buildings to simultaneously control undesirable excessive dynamic responses induced by wind loads and earthquake excitations [5–7].

In order to design and install passive control devices accurately, characteristics of dynamic responses of parallel-placed

adjacent high-rise buildings under wind and earthquake excitations should be investigated to simultaneously control wind- and earthquake-induced vibrations. Unlike earthquake excitations, wind loads acting on the adjacent high-rise buildings may be more complicated [8]. The reason can be mainly attributed to the following two facts: (1) due to the complex interaction of wind and exterior shape of buildings, wind loads include along-wind and across-wind components, which are mainly generated by incoming turbulence and vortex-shedding, respectively [9], and (2) wind loads acting on the target building can be strongly affected by aerodynamic interference if surrounding buildings exist [10–12]. Currently, most of the literature studies are focused on the assessment of structural safety under independent hazards i.e., under earthquakes [13–18] or strong winds [19–22]. However, research interests have been developed amongst engineers and researchers to investigate the design of structures under a combination of extreme multiple hazards [23]. Vulcano [24]

investigated the dynamic responses of a single building with base-isolated devices subjected to strong wind loads and earthquake excitations to pursue the optimal design of the base-isolation system. Hong and Gu [25] found that, in the case of tall flexible buildings whose lateral forces are mainly governed by wind loads, the combined loads after considering wind loads and earthquake excitations may be more unfavourable as compared with those involving wind loads in seismic design. Duthinh and Simiu [26] developed a design approach for buildings in regions where strong winds and earthquakes are significant while satisfying the minimum requirements in design standards. Mahmoud and Cheng [27] proposed a probabilistic framework for estimating the lifecycle cost for two steel buildings subjected to different seismic and wind intensities. Zheng et al. [28] presented a multi-hazard-based framework to assess the damage risk of high-rise buildings subjected to wind and earthquake hazards simultaneously. A comparative study of dynamic responses of liquid storage tanks under wind, earthquake, and combined wind and earthquake excitations is presented by Jing et al. [29]. Their results showed that under strong winds the dynamic responses of the liquid storage tank under wind loads alone are larger than those under earthquake excitations, and the dynamic responses under wind-earthquake interaction are larger than those under wind and earthquake excitations alone. Xu et al. [30] proposed an analytical model for an isolated high-rise building with friction pendulum bearing and magnetorheological damper to reduce dynamic responses under combined wind loads and earthquake excitations. Roy and Matsagar [31] investigated the combined wind and earthquake hazards effects on the failure probability of multistorey steel buildings equipped with passive control devices. Most of the aforementioned studies focused on dynamic responses or failure evaluation of a single building under the simultaneous action of wind and earthquake.

To the best of the authors' knowledge, the comparison between the dynamic responses of adjacent high-rise buildings subjected to wind loads and earthquake excitations has not been thoroughly investigated in the literature. Hence, in the present study, an attempt has been made to investigate the dynamic response characteristics of these parallel-placed linked high-rise buildings to control the structural vibrations under strong wind and earthquake excitations. The present study is arranged as follows: firstly, the equations of motion for the adjacent buildings under the two different kinds of dynamic excitations are established. Subsequently, a structure comprising two adjacent high-rise buildings is briefly introduced considering wind loads obtained from wind tunnel tests and natural earthquake records. Finally, an opposite-sign response factor is identified to compare the displacement, velocity, and acceleration responses of the linked adjacent buildings with different natural frequency ratios under wind loads and earthquake excitations.

2. Mathematical Model of the Adjacent Buildings under Wind and Seismic Excitations

A lumped-mass sketch of adjacent high-rise buildings is shown in Figure 1. The two buildings, named Building 1 (i storeys) and
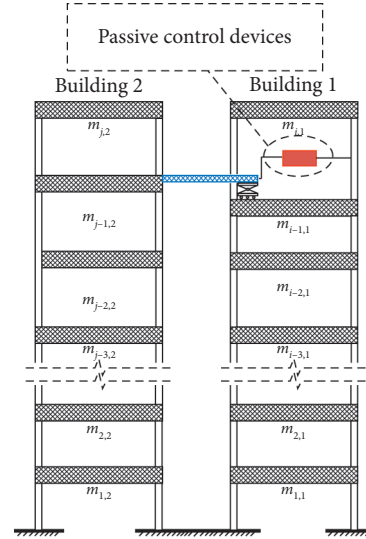

Figure 1: The structural sketch of the two adjacent high-rise buildings.

Building 2 (j storeys), are linked by a corridor with rigid support at one terminal and sliding support at the other terminal. Different passive control devices may be installed at the storey having the same intermediate height as that of the corridor to mitigate the dynamic responses when these responses do not satisfy the requirement of design standards. These different types of passive control devices can be categorized into displacement-dependent such as metal friction dampers [32, 33] or buckling-restrained braces [34], velocity-dependent such as fluid viscous dampers [35–39], or acceleration-dependent primarily related to inerter devices [40–42]. Therefore, while selecting suitable passive control devices, the dynamic response characteristics of the adjacent high-rise buildings under wind loads and seismic excitations should be fully considered to obtain a better mitigation efficiency of these devices.

The equations of motion of adjacent high-rise buildings without any passive control devices under wind loads and seismic excitations can be expressed as in equations (1) and (2), respectively.

$$\mathbf{M}\ddot{\mathbf{X}}(t) + \mathbf{C}\dot{\mathbf{X}}(t) + \mathbf{K}\mathbf{X}(t) = \mathbf{P}(t), \tag{1}$$

$$\mathbf{M}\ddot{\mathbf{X}}(t) + \mathbf{C}\dot{\mathbf{X}}(t) + \mathbf{K}\mathbf{X}(t) = -\mathbf{M}\{1\}\ddot{x}_g(t), \tag{2}$$

where, $\mathbf{M}$, $\mathbf{C}$, and $\mathbf{K}$ are the mass, damping, and stiffness matrices of the two adjacent high-rise buildings, respectively. The lumped mass and lateral stiffness of each storey can be obtained from the finite element model of the buildings. $\ddot{\mathbf{X}}(t)$, $\dot{\mathbf{X}}(t)$, and $\mathbf{X}(t)$ correspond to the acceleration, velocity, and displacement column vectors of adjacent high-rise buildings, respectively. $\mathbf{P}(t)$ is the wind load vector acting on the center of mass of each storey, which can be obtained from wind tunnel tests of synchronous multipoint pressure measurements. $\ddot{x}_g(t)$ is the acceleration of ground motion at time t, and $\{1\}$ is a column vector with $(i + j)$entries, in which all entries are equal to 1.

The mass matrix $\mathbf{M}$ can be expressed as

$$\mathbf{M} = \text{diag}\left[m_{1,1}, m_{2,1} \ldots, m_{i,1}, m_{1,2}, m_{2,2} \ldots, m_{j,2}\right], \quad (3)$$

where $m_{i,1}$ and $m_{j,2}$ denote the dead and live loads (properly combined with each other) of the ith storey of Building 1 and the jth storey of Building 2, respectively.

The stiffness matrix $\mathbf{K}$ can be defined as

$$\mathbf{K} = \begin{bmatrix} \mathbf{K}_{i \times i,1} & 0 \\ 0 & \mathbf{K}_{j \times j,2} \end{bmatrix}, \quad (4)$$

where $\mathbf{K}_{i \times i,1}$ and $\mathbf{K}_{j \times j,2}$ represent the stiffness matrix of original Building 1 and Building 2, respectively.

The damping matrix $\mathbf{C}$ can be expressed according to the Rayleigh formulation:

$$\mathbf{C}_{(i+j) \times (i+j)} = a_0 \mathbf{M}_{(i+j) \times (i+j)} + a_1 \mathbf{K}_{(i+j) \times (i+j)}, \quad (5)$$

where a_0 and a_1 are two scalar coefficients of proportionality.

Since the mass, damping, and stiffness matrices are orthogonal to the mode shape, equations (1) and (2) can be decoupled into the modal coordinates as expressed in equations (6) and (7), respectively.

$$\ddot{q}_k(t) + 2\xi_k \omega_k \dot{q}_k(t) + \omega_k^2 q_k(t) = \frac{P_k^*(t)}{M_k^*}, \quad (6)$$

$$\ddot{q}_k(t) + 2\xi_k \omega_k \dot{q}_k(t) + \omega_k^2 q_k(t) = -\left(\frac{-\{\phi_k\}^T \mathbf{M}\{1\}}{\{\phi_k\}^T \mathbf{M}\{\phi_k\}}\right)\ddot{x}_g, \quad (7)$$

where $q_k(t)$, ξ_k, ω_k, $P_k^*(t)$, M_k^*, and ϕ_k denote the kth order generalized coordinates, damping ratio, natural circular frequency, generalized aerodynamic force, and generalized mass, vibration mode, respectively. The superscript T denotes the transpose operator, and the modal participation coefficient γ_k is defined as

$$\gamma_k = \frac{\{\phi_k\}^T \mathbf{M}\{1\}}{\{\phi_k\}^T \mathbf{M}\{\phi_k\}}. \quad (8)$$

The time-domain integration method, i.e., Duhamel's integral, is used to solve the generalized coordinate $q_k(t)$ under wind and earthquake excitations, which are formulated as in equations (9) and (10), respectively.

$$q_k(t) = \frac{1}{M_k^* \omega_{dk}} \int_0^t P_k^*(\tau) e^{-\xi_k \omega_k (t-\tau)} \sin \omega_{dk}(t-\tau) d\tau, \quad (9)$$

$$q_k(t) = -\left(\frac{1}{\omega_{dk}}\right) \int_0^t \gamma_k \ddot{x}_g(\tau) e^{-\xi_k \omega_k (t-\tau)} \sin \omega_{dk}(t-\tau) d\tau, \quad (10)$$

where ω_{dk} is the kth damped natural frequency of the structure.

According to the modal superposition method, the displacement response of the structure at arbitrary t can be expressed as

$$\{x(t)\} = \sum_{k=1}^{N} \{\phi_k\} q_k(t), \quad (11)$$

where N is the number of the mode shape involved while calculating the displacement time history of the structure.

3. Case Study

The following section introduces a case study of two adjacent high-rise buildings and the related excitations to evaluate the dynamic responses: in particular, wind loads are obtained from wind tunnel tests of synchronous multipoint pressure measurements, while 44 natural ground-motion records are considered for earthquake-induced excitations.

3.1. A Brief Introduction of the Two Adjacent High-Rise Buildings. The same structure previously considered by De Domenico et al. [43] is analyzed as a case, comprising two adjacent high-rise buildings whose main properties are summarized as follows. Building 1 has 59 storeys with 268 meters height and Building 2 consists of 55 storeys with a height of 210.2 meters. The main dimensions of the adjacent buildings and the definition of the coordinate system for structural analysis and wind directions are shown in Figures 2(a) and 2(b).

The distribution of lumped masses of the two buildings is presented in Figure 3(a)The lateral stiffness along the x-axis of two buildings is smaller than that along the y-axis; as a result, the most unfavourable dynamic response will probably occur along the x-axis. Hence, only lateral stiffness along the x-axis is plotted in Figure 3(b).

According to the mass and stiffness matrices of the individual adjacent buildings, the fundamental frequencies of Building 1 and Building 2 are obtained. The first five natural frequencies of the individual buildings are listed in Table 1. As shown in Table 1, the natural frequency ratio (NFR) which is defined as the ratio of the first natural frequency of Building 1 to that of Building 2 can be estimated as 0.86/1. To investigate the effects of natural frequency ratio on dynamic responses of adjacent buildings under different excitations, the mass of Building 2 is adjusted so as to make its first natural frequency equal to that of Building 1, which means that the natural frequency ratio is equal to 1/1.

3.2. Wind Tunnel Test and Ground-Motion Time Histories. Wind tunnel tests of synchronous multipoint pressure measurement are carried out in the wind tunnel laboratory of Shantou University. The scale ratio of the test model to the prototype of the buildings is 1 : 300. In the wind tunnel tests, the B-type wind field is simulated according to the Chinese building code [45]. The wind tunnel tests are conducted for 24 wind directions ranging from 0° to 345° at an interval of 15° to investigate the effect of wind direction on the dynamic responses of the structure. For the displacement and acceleration responses of the buildings, the basic wind pressures are assumed to be 0.6 kPa and 0.35 kPa (corresponding to 50-year and 10-year return periods, respectively). More
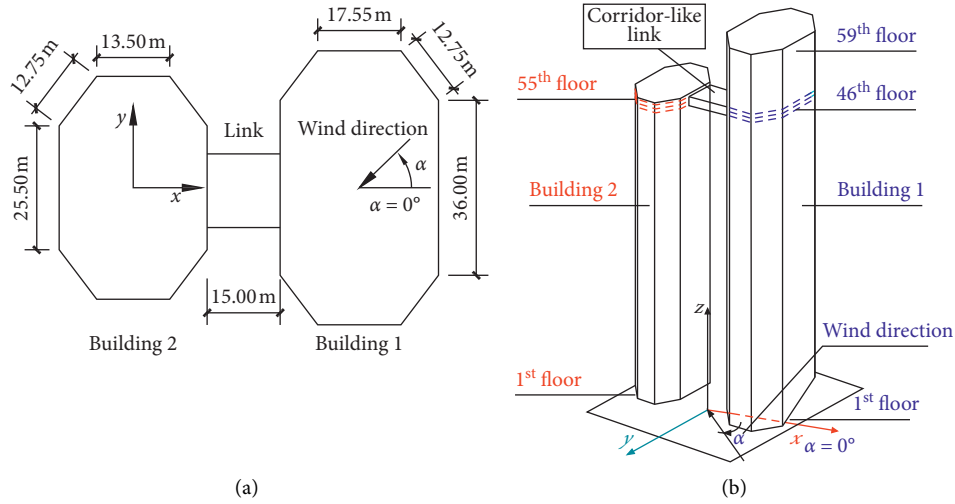
(a)

(b)

Figure 2: (a) Plane view of adjacent buildings and definition of the coordinate system and wind direction [8] and (b) axonometric sketch of two buildings [43].
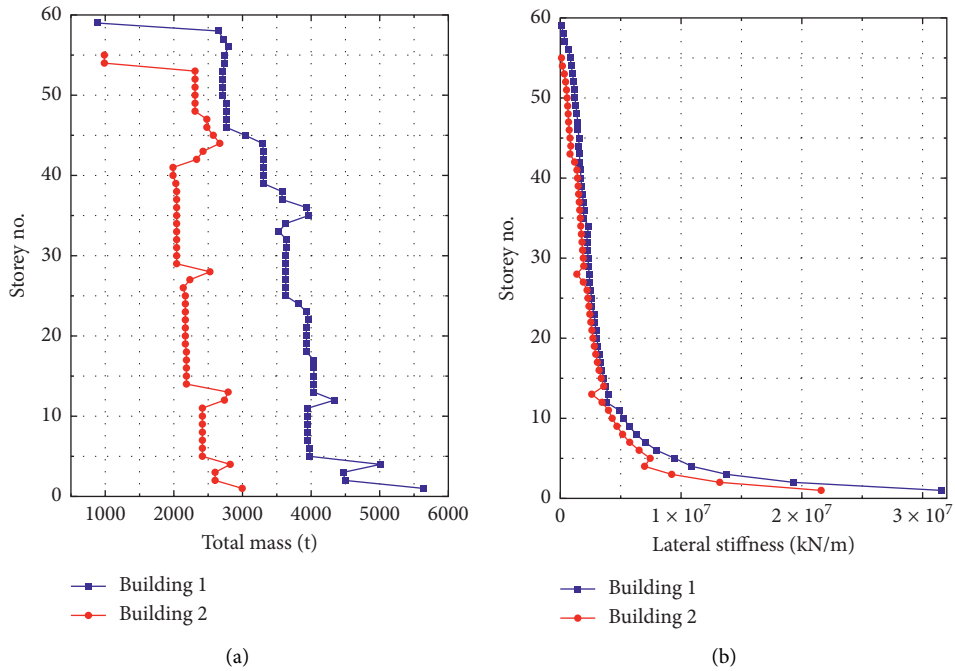

(a)

(b)

Figure 3: Distribution of (a) lumped masses and (b) lateral stiffness of the two buildings along the x-axis [44].

Table 1: Natural frequencies of individual buildings.

Frequency (Hz)	f_1	f_2	f_3	f_4	f_5
Building 1	0.139	0.347	0.554	0.756	0.959
Building 2	0.161	0.399	0.636	0.866	1.090

detailed information about the wind tunnel test can be found in the literature [44].

Based on the results obtained from wind tunnel tests, the normalized power spectral density (PSD) of base shear forces on Building 1 and Building 2 at across-wind direction is plotted in Figure 4. The PSD curves of Building 1 and Building 2 have obvious peaks corresponding to the dimensionless values $f B/U_H = 0.107$ and 0.120, where f represents frequency measuring by Hz, B is width of the individual building, U_H denotes mean wind speed at top of the buildings corresponding to 50-year return period, and $S(f)$ and σ_z represent self-power spectrum and root mean square of the base shear forces, respectively.

With regard to the earthquake excitation, the dynamic responses of adjacent high-rise buildings are evaluated under 44 natural ground-motion records, which are two horizontal components of 22 earthquakes obtained from the FEMA P-695 far-field record set [46]. Some seismological information of the 22 earthquakes is listed in Table 2. These ground-motion records have been used in previous
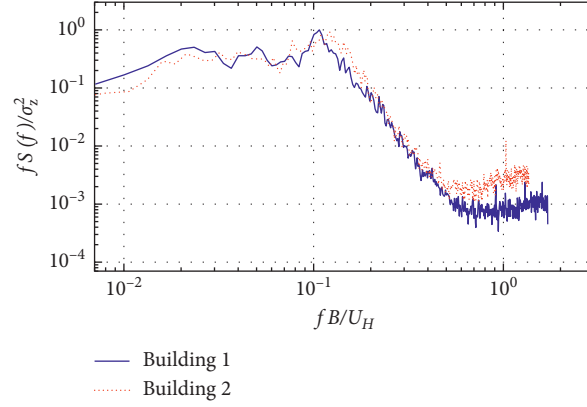
FIGURE 4: Normalized PSD of base shear forces at the across-wind direction.

TABLE 2: Information of 22 considered earthquakes from FEMA P-695 far-field record set [46].

ID no.	Earthquake			Recording station	
	Magnitude	Year	Name	Name	Owner
1	6.7	1994	Northridge	Beverly Hills-Mulhol	USC
2	6.7	1994	Northridge	Canyon Country-WLC	USC
3	7.1	1999	Duzce, Turkey	Bolu	ERD
4	7.1	1999	Hector Mine	Hector	SCSN
5	6.5	1979	Imperial Valley	Delta	UNAMUCSD
6	6.5	1979	Imperial Valley	El Centro Array #11	USGS
7	6.9	1995	Kobe, Japan	Kobe, Japan	CUE
8	6.9	1995	Kobe, Japan	Shin-Osaka	CUE
9	7.5	1999	Kocaeli, Turkey	Duzce	ERD
10	7.5	1999	Kocaeli, Turkey	Arcelik	KOERI
11	7.3	1992	Landers	Yermo Fire Station	CDMG
12	7.3	1992	Landers	Coolwater	SCE
13	6.9	1989	Loma Prieta	Capitola	CDME
14	6.9	1989	Loma Prieta	Gilroy Array #3	CDMG
15	7.4	1990	Manjil, Iran	Abbar	BHRC
16	6.5	1987	Superstition Hills	El Centro Imp. Co.	CDMG
17	6.5	1987	Superstition Hills	Poe Road (Temp)	USGS
18	7.0	1992	Cape Mendocino	Rio Dell Overpass	CDMG
19	7.6	1999	Chi-Chi, Taiwan	CHY101	CWB
20	7.6	1999	Chi-Chi, Taiwan	TCU045	CWB
21	6.6	1971	San Fernando	LA-Hollywood Stor	CDMG
22	6.5	1976	Friuli, Italy	Tolmezzo	--

researches to investigate the mitigation effects of different passive control devices [47, 48]. The individual and average PSDs of 44 recorded earthquakes are shown in Figure 5. It is observed that the predominant frequencies of these earthquake excitations concentrate on a higher frequency range as compared to those of wind loads as shown in Figure 4.

4. Dynamic Response Analysis of Adjacent Buildings under Wind and Earthquake Excitations

According to the mathematical model described in Section 2, wind loads and earthquake excitations in Section 3, the time history of displacement, velocity, and acceleration response for the adjacent high-rise buildings under wind loads and seismic excitations are estimated numerically. To quantitatively compare these response characteristics, an opposite-sign response factor F_{opp} is introduced in this study, which is defined as

$$F_{\text{opp}} = \frac{T_{\text{opp}}}{T_{\text{total}}} \times 100\%, \tag{12}$$

where T_{opp} is the sum of the time intervals during which fluctuating components of wind-induced displacement responses or, similarly, total velocity and acceleration responses of buildings (the mean values of velocity and acceleration responses are equal to zero) have opposite sign, and T_{total} is the total statistical time of dynamic responses.

4.1. Comparison of Displacement Responses. According to equation (1) to equation (11), the time histories of dynamic displacement responses of adjacent high-rise buildings under wind loads and earthquake excitations are evaluated.
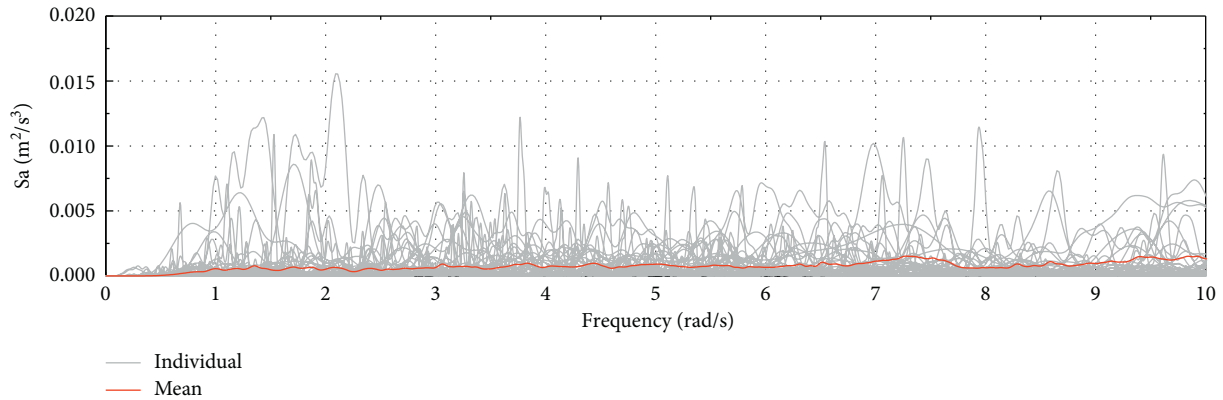
FIGURE 5: The individual and mean PSDs of the 44 recorded earthquakes belonging to the FEMA P695 far-field record set [40].

The total wind-induced responses of structures can be decomposed into mean value and fluctuating components. Previous literature [8, 43, 44, 49, 50] showed that the passive control devices can only suppress the fluctuating vibration, thus while investigating dynamic response characteristics, only the fluctuating response is analyzed. For the clarity of the figures, Figure 6 shows only the 50-second segment of fluctuating displacement time history of the adjacent high-rise buildings and the shaded part indicates that the direction of displacement of the two buildings is opposite; i.e., if the sign of one response is negative, the other sign is positive. Figures 6(a)–6(c) illustrate the time history of the wind-induced fluctuating displacement responses at the height of 210.2 meters of the adjacent buildings with a natural frequency ratio of 0.86/1 at 0°, 90°, and 180° wind directions, respectively. Figure 6(d) presents the time history of displacement for the adjacent buildings at the height of 210.2 meters under the No. 10 earthquake excitation.

Once the time histories of wind-induced and earthquake-induced displacement responses are obtained, the opposite-sign displacement factor of the adjacent buildings at the height of 210.2 meters may be estimated according to equation (12). The total statistical time for seismic responses is the same as recorded time of each ground motion, while that of wind-induced responses is set to be 600 seconds. The variations of opposite-sign displacement factor with wind directions and different seismic excitations are shown in Figure 7. The red dashed line in the figure represents the mean value of factors of wind directions and earthquake excitations, respectively. Figure 7(a) indicates that wind-induced opposite-sign displacement factor hardly varies with wind directions, while it is nearly not affected by the natural frequency ratio. Figure 7(b) indicates that the opposite-sign factor of the two buildings with the natural frequency ratio of 0.86/1 is much larger than that with the natural frequency ratio of 1/1 under the majority of seismic excitations. The mean value (for all the 44 seismic records) of the opposite-sign displacement response factor is 36.5% when the natural frequency ratio is 0.86/1, and it is reduced to 11.1% when the natural frequency ratio is 1/1.
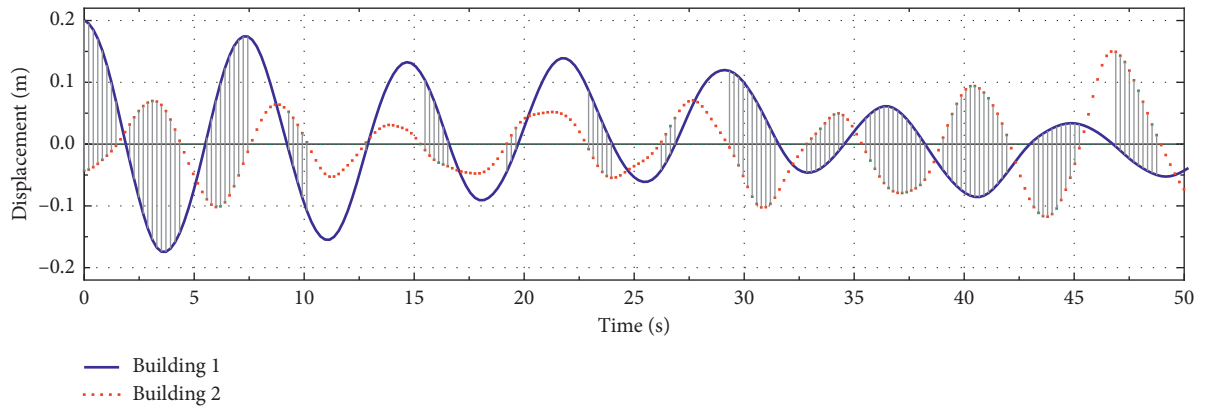
Figure 8 shows the variation of opposite-sign displacement factor with the height of buildings under wind and seismic excitations. Figure 8(a) indicates that the factors under the four wind directions do not vary significantly with the height of the buildings and are insensitive to the natural frequency ratio. Figure 8(b) illustrates that the mean value of the opposite-sign factor of the two buildings subjected to seismic excitations is much smaller when the natural frequency ratio is equal to 1/1 than that when the natural frequency ratio is equal to 0.86/1 at any height of the two buildings.

4.2. Comparison of Velocity Responses. The velocity response time histories can be obtained from the derivative of the displacement time histories with respect to time. Figures 9(a) and 9(b) show the time histories of velocity response at a height of 210.2 meters of the two buildings with the natural frequency ratio being 0.86/1 under across-wind direction (90°) and the No. 10 seismic excitation, respectively. The shaded part in Figure 9 means that the velocity responses of the two buildings have the opposite sign.

The variations of the opposite-sign velocity factor with different wind directions and earthquake excitations are shown in Figure 10. Figure 10(a) indicates that the wind-induced velocity factors are insensitive to wind directions and natural frequency ratios of the two buildings since all the values of factors approach around 50% under 24 wind directions and different natural frequency ratios. Figure 10(b) illustrates that factors related to velocity responses under seismic excitations are sensitive to natural frequency ratio of the two buildings. Under most of the seismic excitations, the factors are relatively lower when the natural frequency ratio is 1/1 than that at the condition of the natural frequency ratio being 0.86/1. The mean values of the opposite-sign factors for seismic excitation are 40.3% and 25.0% corresponding to natural frequency ratios of 0.86/1 and 1/1, respectively.

Figure 11 presents the variation of the opposite-sign velocity factor with the varying height of the two buildings under wind loads and earthquake excitations, respectively. Figure 11(a) illustrates that the factors remain steady with the varying height and natural frequency ratio of the two adjacent buildings, and these values of factors lie around 50% at the four typical wind directions. Figure 11(b) indicates that the mean value of the velocity
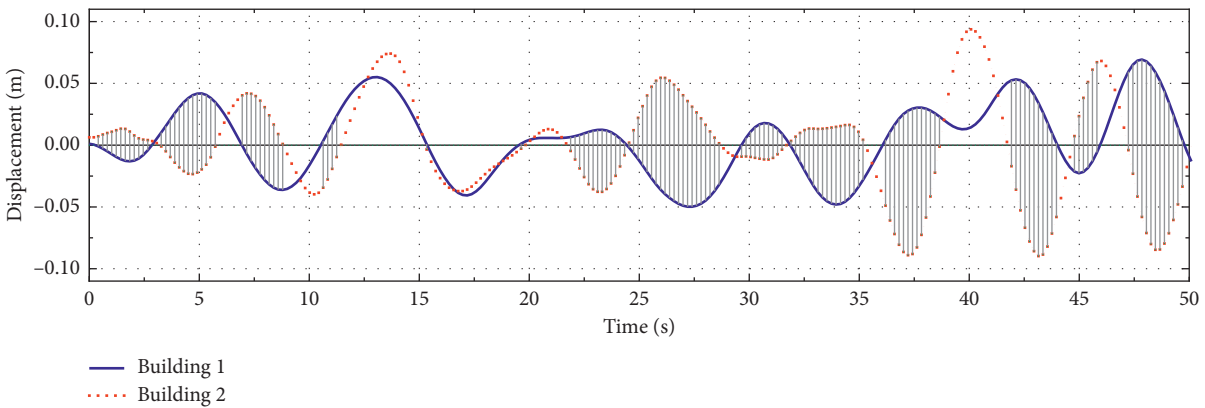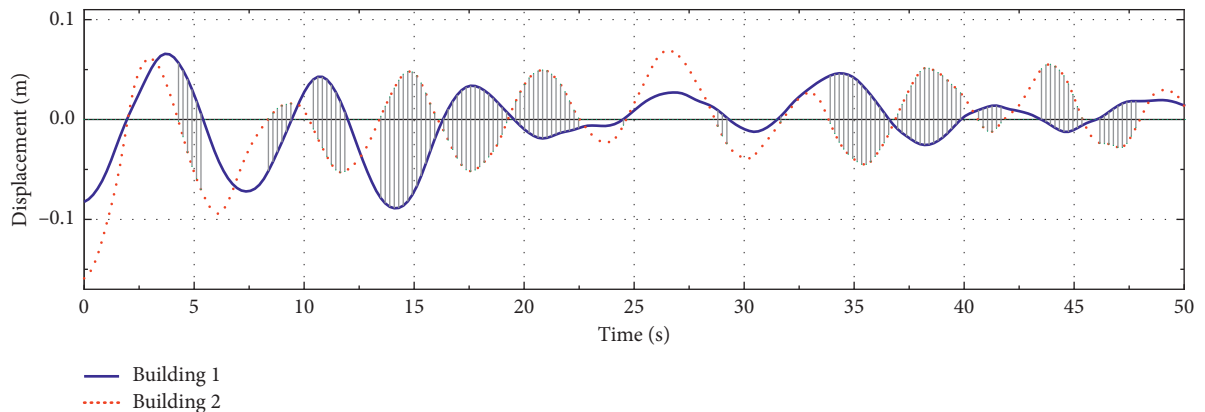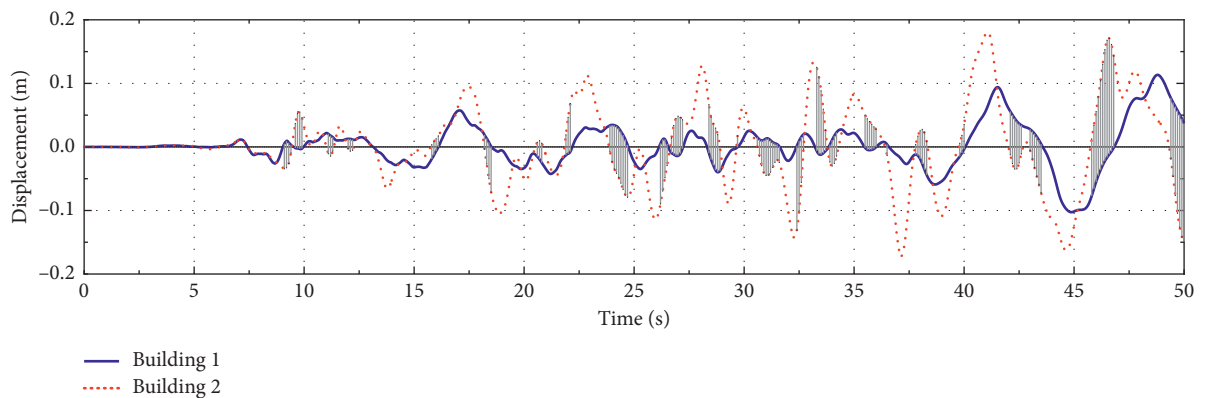
Figure 6: Time histories of displacement responses at 210.2 m height under (a) 0° wind direction, (b) 90° wind direction, (c) 180° wind direction, and (d) the No. 10 earthquake excitation.
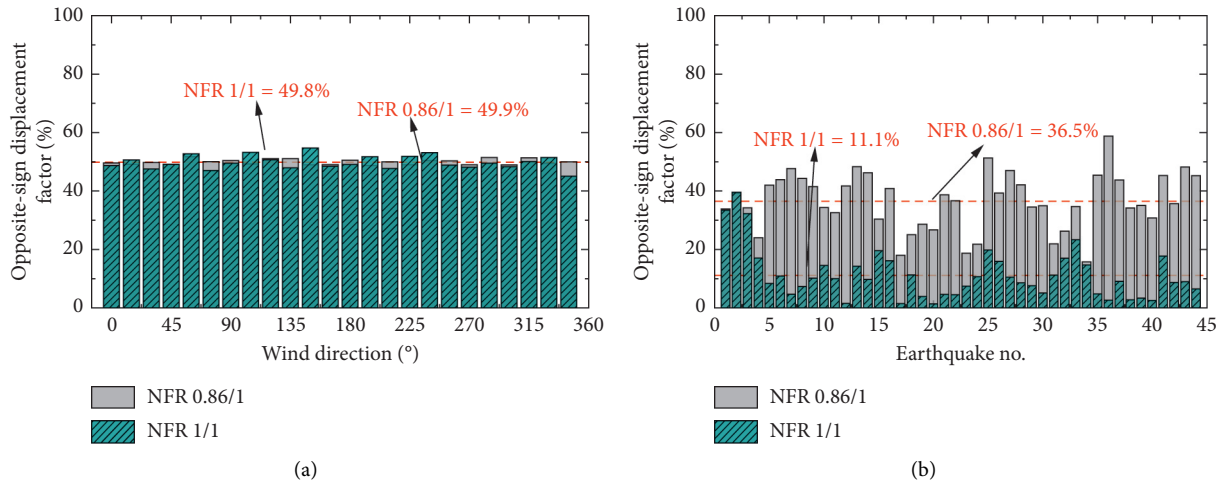
FIGURE 7: Variation of opposite-sign displacement factor at 210.2 m height under (a) 24 wind directions and (b) 44 earthquake excitations.
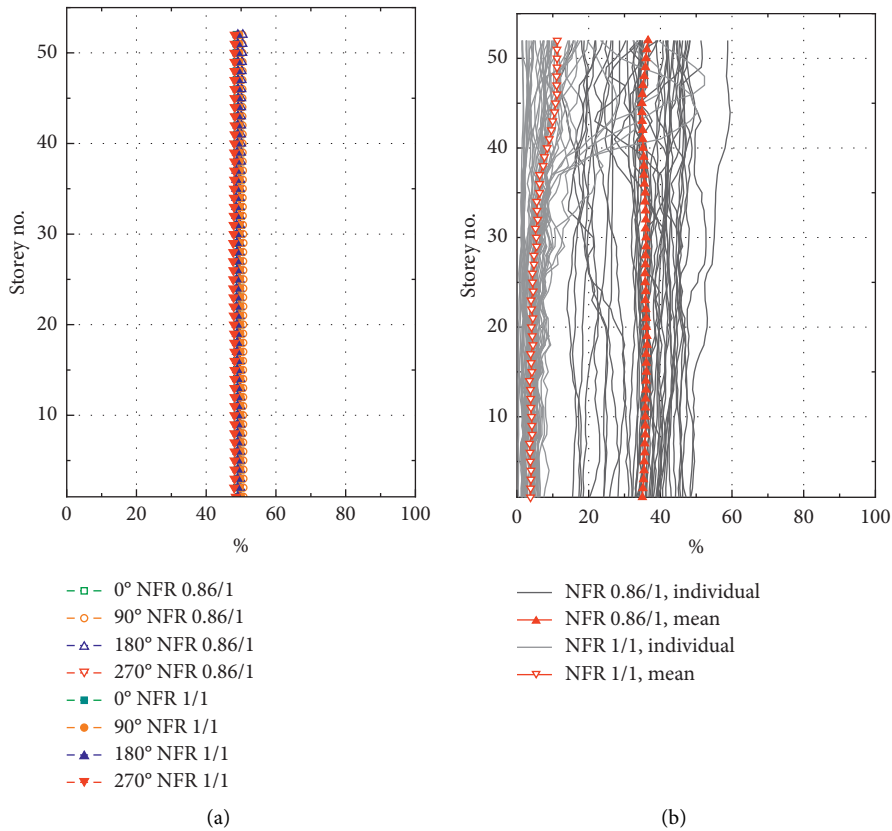

FIGURE 8: Variation of opposite-sign displacement factor with height of buildings under (a) wind loads and (b) 44 earthquake excitations.

factor of the two buildings in the case of natural frequency being 0.86/1 is larger than that when natural frequency ratio is 1/1 at any height of the two buildings under seismic excitations.

4.3. Comparison of Acceleration Responses. The acceleration response time histories of the adjacent buildings under wind loads and seismic excitations are estimated in this section. Figures 12(a) and 12(b) show a 50-second time history of
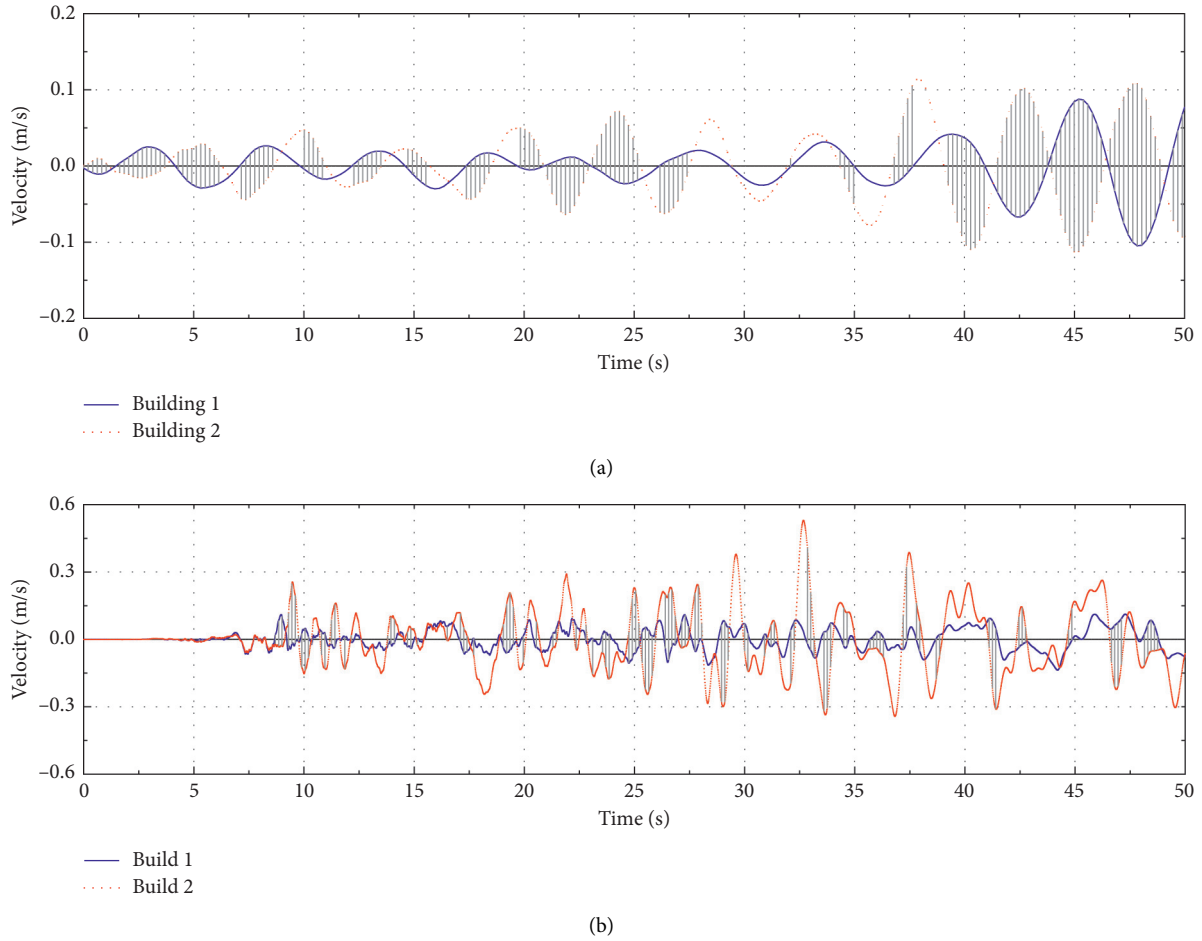
(a)

(b)

FIGURE 9: Time histories of velocity responses at 210.2 m height under (a) 90° wind direction and (b) the No. 10 earthquake excitation.
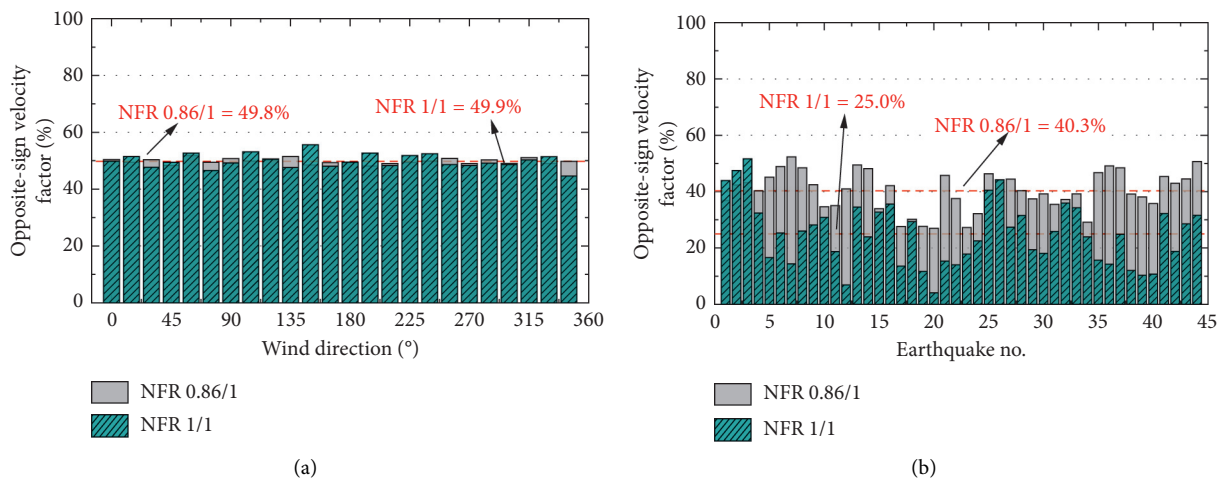

(a)

(b)

FIGURE 10: Variation of opposite-sign velocity factor at 210.2 m height under (a) 24 wind directions and (b) 44 earthquake excitations.

acceleration responses of the two buildings under the across-wind direction (90°) and the No. 10 earthquake excitation respectively.

Figure 13 shows the variation of the opposite-sign acceleration response factor with different wind directions and earthquake excitations. Figure 13(a) indicates that the wind-
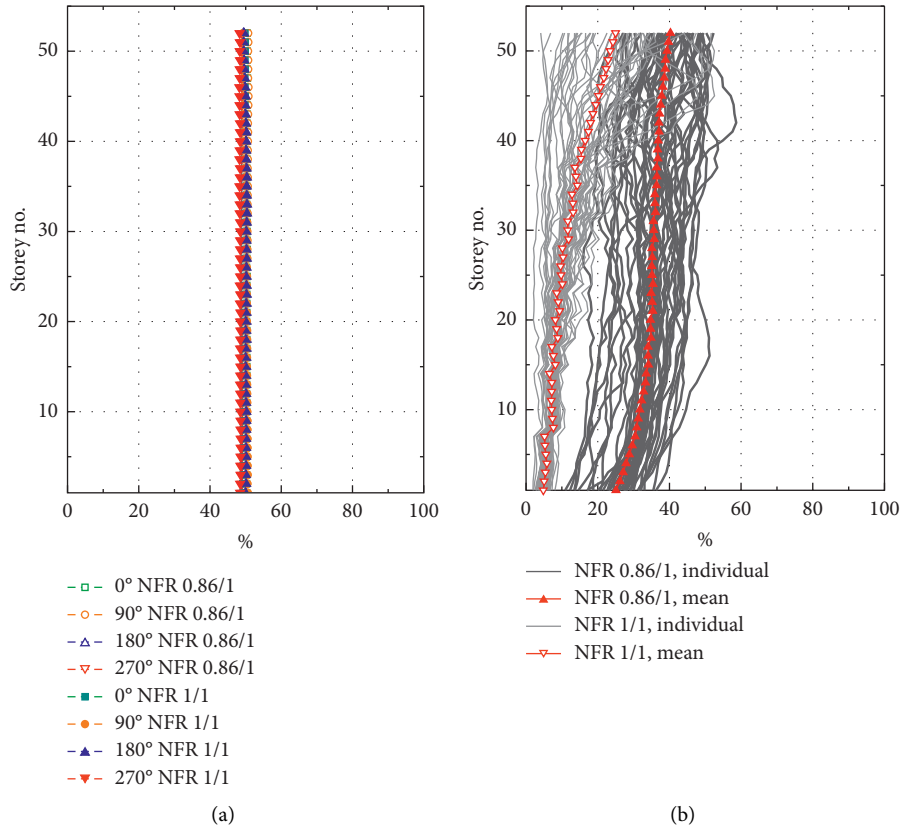
(a)

(b)

FIGURE 11: Variation of opposite-sign velocity factor with height of buildings under (a) wind loads and (b) 44 earthquake excitations.
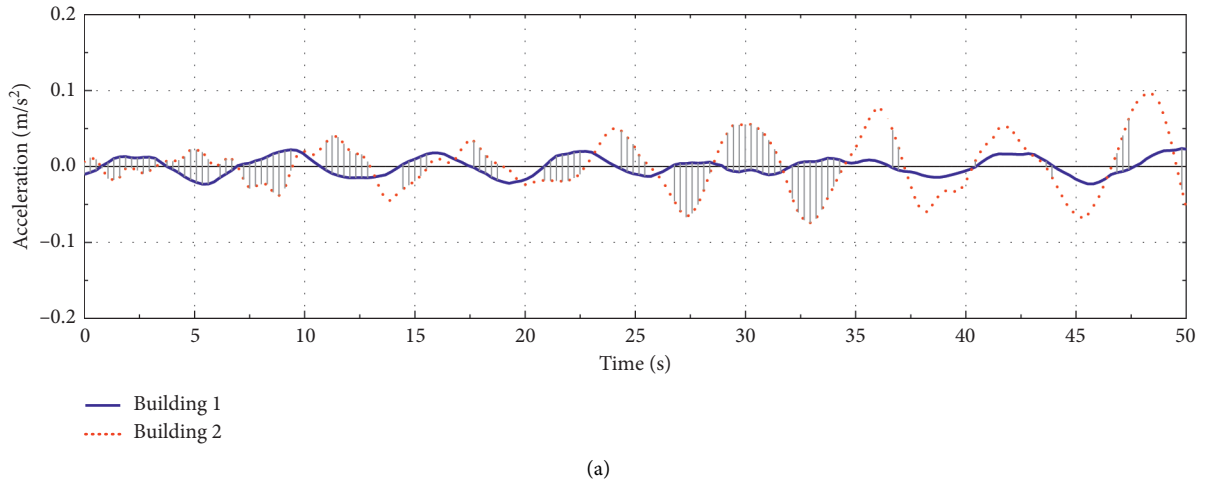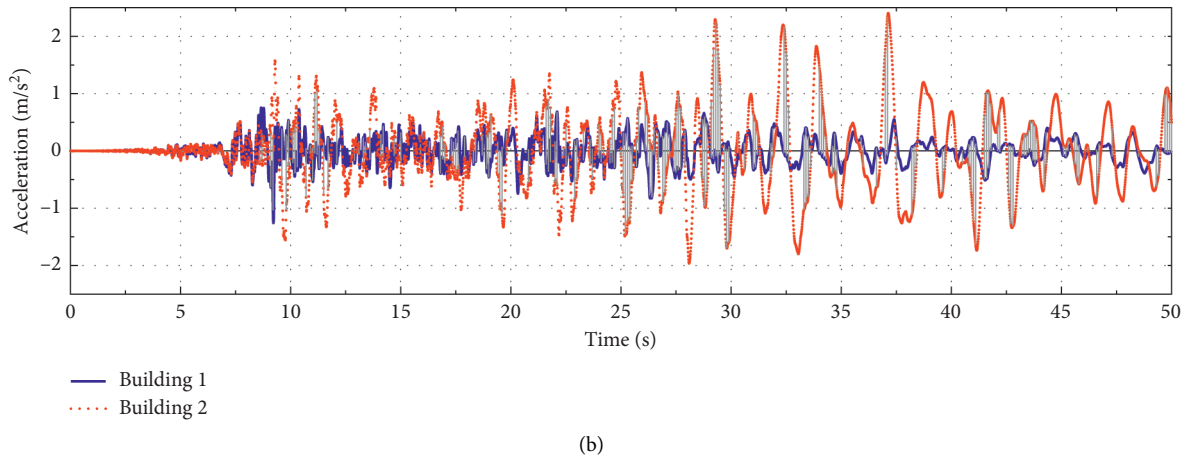

(a)

FIGURE 12: Continued.

(b)

FIGURE 12: Time histories of acceleration responses at 210.2 m height under (a) 90° wind direction and (b) the No. 10 earthquake excitation.
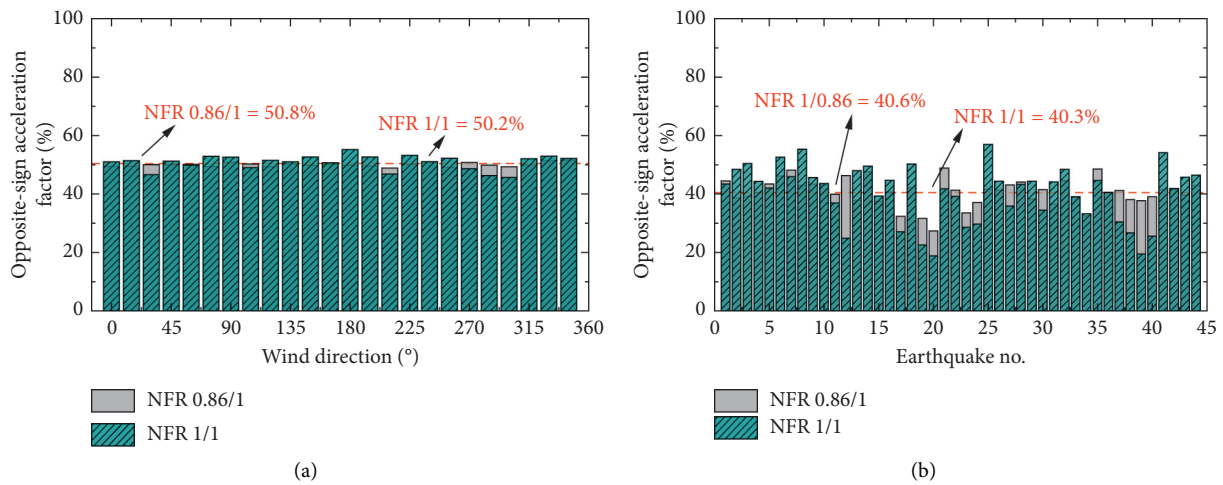

(a)

(b)

FIGURE 13: Variation of opposite-sign acceleration factor at 210.2 m height under (a) 24 wind directions and (b) 44 earthquake excitations.

induced acceleration response factor remains almost invariant while changing wind directions and natural frequency ratio of adjacent buildings, and the mean value for all wind directions in each working condition still lies around 50%. As for earthquake excitations, Figure 13(b) demonstrates that the variation of the earthquake-induced acceleration response factors caused by the changes in natural frequency ratio is not as significant as that of the displacement or velocity response factor shown in Figures 7(b) and 10(b), respectively. The mean value of the opposite-sign acceleration response factor under the 44 earthquake excitations is 40.6% when the natural frequency ratio is 0.86/1, while the factor is 40.3% when natural frequency ratio equals to 1/1.

Figure 14 presents the variation of opposite-sign acceleration response factor with the height of two buildings under wind and seismic excitations. Figure 14(a) shows that

the acceleration response factors are almost unaffected with the changing height of the building and natural frequency ratios of the two buildings at the four wind directions, which is similar to the variation of wind-induced velocity response factor with height as shown in Figure 11(a). With regard to the seismic excitation, Figure 14(b) indicates that the acceleration response factors at the top storeys of the adjacent buildings with natural frequency ratio of 1/1 are equal to the case when natural frequency ratio is 0.86/1.

5. Conclusion and Discussion

In the present work, an opposite-sign response factor is proposed to compare the characteristics of the dynamic responses of two adjacent high-rise buildings under wind loads and earthquake excitations, respectively. This factor is defined as the ratio between the time duration during which
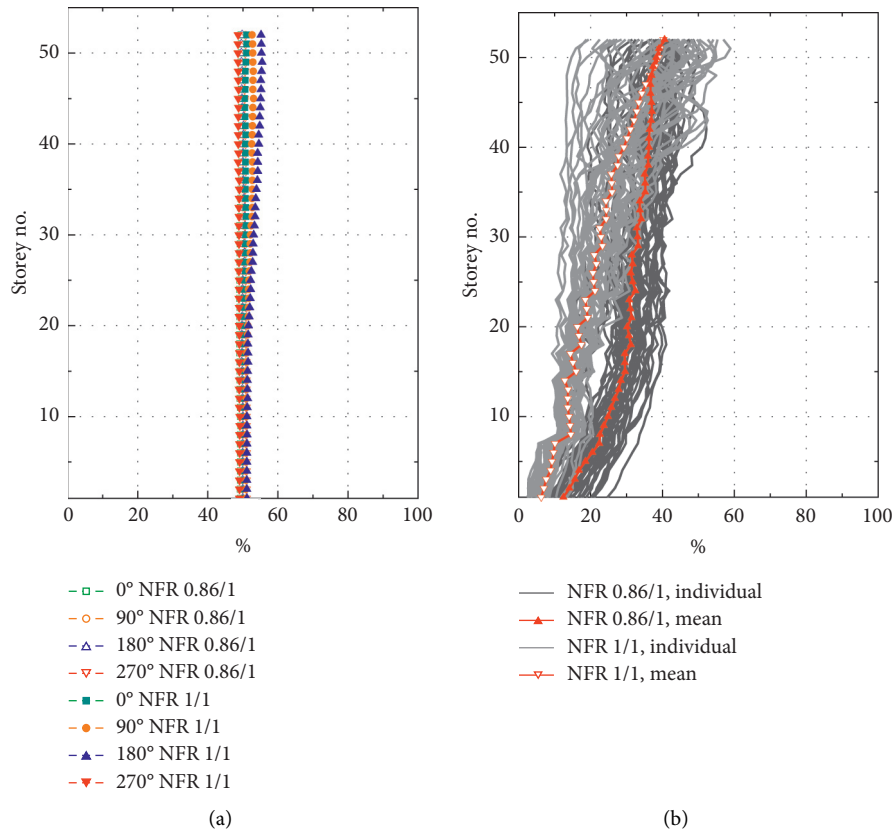
FIGURE 14: Variation of opposite-sign acceleration factor with height of buildings under (a) wind loads and (b) 44 earthquake excitations.

dynamic responses of the adjacent buildings have the opposite sign and the total statistical time of dynamic responses. The following conclusions are obtained as a result of the present research.

(1) For fluctuating displacement responses, the opposite-sign displacement response factors vary more significantly with different earthquake excitations than that under different wind directions. Besides, these factors of seismic excitations are more sensitive to changes in the natural frequency ratio of the two buildings as compared to wind loads.

(2) In terms of the velocity responses, the opposite-sign velocity response factors remain almost constant with change in both wind directions and the natural frequency ratio of the two buildings, under wind loads. However, under earthquake excitations, these factors vary with different earthquake records and natural frequency ratios. Furthermore, the mean value of the wind-induced factor is larger than that obtained under 44 seismic factors.

(3) Regarding acceleration responses, results of wind-induced opposite-sign acceleration factors are similar to those of wind-induced velocity responses, and the mean values of wind-induced acceleration factors are also larger than those of 44 seismic excitations. Nevertheless, the seismic acceleration factors do not

vary significantly with different earthquake records and natural frequency ratios as compared to that of seismic displacement and velocity responses.

In general, the opposite-sign dynamic response factors of the adjacent buildings under the action of wind loads are larger than those under earthquake excitations. This result implies that when inter-building passive control devices are installed to mitigate dynamic responses of the two adjacent high-rise buildings, the mitigation efficiency of the devices for wind-induced vibration control is better than the seismic vibration control. This anticipation is consistent with the previous works [8, 43, 44, 48] from the authors dealing with wind-induced and earthquake-induced vibration mitigation with inter-building passive control devices. In these researches, different acceleration-dependent tuned inerter dampers, i.e., TMDI and TLCDI, were employed to control wind-induced and seismic responses of the two adjacent high-rise buildings analyzed in the present work. After the installation of TMDI on the two adjacent buildings, the mean reduction coefficients of the top-level acceleration are 37.5% for Building 1 and 45.2% for Building 2 at the across-wind direction, while the maximum corresponding reduction coefficients under seismic excitations are only 23.0% and 37.5% [43, 44]. If TLCDI is installed to mitigate dynamic responses, the reduction coefficients of wind-induced acceleration responses of Building 1 and Building 2 are 37.7% and 42.0%, respectively, while the corresponding reduction coefficients in case of seismic acceleration control

are only 15.7% and 26.1% [8, 48]. These findings verify that both TMDI and TLCDI are more effective in controlling the wind-induced acceleration responses of adjacent high-rise buildings, as compared to earthquake-induced acceleration responses. Hence, the opposite-sign response factor analyzed in this study could be regarded as an applicable and reasonable indicator to evaluate the mitigation efficiency of passive control devices even prior to their installation.

Data Availability

The data used to support the findings of this research are available from the corresponding author upon request.

Conflicts of Interest

The authors declare that they have no conflicts of interest.

Acknowledgments

References

[1] K. Al-Kodmany, "Skyscrapers in the twenty-first century city: a global snapshot," *Buildings*, vol. 8, no. 12, p. 175, 2018.

[2] G. Hu, K. T. Tse, J. Song, and S. Liang, "Performance of wind-excited linked building systems considering the link-induced structural coupling," *Engineering Structures*, vol. 138, pp. 91–104, 2017.

[3] B. Kavyashree, S. Patil, and V. S. Rao, "Review on vibration control in tall buildings: from the perspective of devices and applications," International Journal of Dynamics and Control, pp. 1–16, 2020.

[4] Q. Wang, H. Qiao, W. Li, Y. Yugen, Z. Fan, and N. Deep Tiwari, "Parametric optimization of an inerter-based vibration absorber for wind-induced vibration mitigation of a tall building," *Wind and Structures*, vol. 31, no. 3, pp. 241–253, 2020.

[5] D.-G. Lee, H.-S. Kim, and H. Ko, "Evaluation of coupling-control effect of a sky-bridge for adjacent tall buildings," *The Structural Design of Tall and Special Buildings*, vol. 21, no. 5, pp. 311–328, 2012.

[6] L.-S. Fur, H. T. Y. Yang, and S. Ankireddi, "Vibration control of tall buildings under seismic and wind loads," *Journal of Structural Engineering*, vol. 122, no. 8, pp. 948–957, 1996.

[7] C. Christopoulos and M. Montgomery, "Viscoelastic coupling dampers (VCDs) for enhanced wind and seismic performance of high-rise buildings," *Earthquake Engineering & Structural Dynamics*, vol. 42, no. 15, pp. 2217–2233, 2013.

[8] Q. Wang, H. Tian, H. Qiao, N. D. Tiwari, and Q. Wang, "Wind-induced vibration control and parametric optimization of connected high-rise buildings with tuned liquid-column-damper-inerter," *Engineering Structures*, vol. 226, Article ID 111352, 2021.

[9] E. Simiu and D. Yeo, *Wind Effects on Structures: Modern Structural Design for Wind*, John Wiley & Sons, Hoboken, NJ, USA, 2019.

[10] W. Kim, Y. Tamura, and A. Yoshida, "Interference effects on local peak pressures between two buildings," *Journal of Wind Engineering and Industrial Aerodynamics*, vol. 99, no. 5, pp. 584–600, 2011.

[11] X. F. Yu, Z. N. Xie, X. Wang, and B. Cai, "Interference effects between two high-rise buildings on wind-induced torsion," *Journal of Wind Engineering and Industrial Aerodynamics*, vol. 159, pp. 123–133, 2016.

[12] X. Yu, Z. Xie, and M. Gu, "Interference effects between two tall buildings with different section sizes on wind-induced acceleration," *Journal of Wind Engineering and Industrial Aerodynamics*, vol. 182, pp. 16–26, 2018.

[13] H.-S. Kim, "Seismic response control of adjacent buildings coupled by semi-active shared TMD," *International Journal of Steel Structures*, vol. 16, no. 2, pp. 647–656, 2016.

[14] W. Shen, A. Niyitangamahoro, Z. Feng, and H. Zhu, "Tuned inerter dampers for civil structures subjected to earthquake ground motions: optimum design and seismic performance," *Engineering Structures*, vol. 198, Article ID 109470, 2019.

[15] S. Mahmoud, "Horizontally connected high-rise buildings under earthquake loadings," *Ain Shams Engineering Journal*, vol. 10, no. 1, pp. 227–241, 2019.

[16] E. Tubaldi, L. Gioiella, F. Scozzese, L. Ragni, and A. Dall'Asta, "A design method for viscous dampers connecting adjacent structures," *Frontiers in Built Environment*, vol. 6, p. 25, 2020.

[17] A. Bhaskararao and R. Jangid, "Seismic response of adjacent buildings connected with dampers," in *Proceedings of the 13th World Conference on Earthquake Engineering*, Vancouver, Canada, August 2004.

[18] S.-Y. Ok, "Tuned mass damper asymmetric coupling system for vibration control of adjacent twin buildings," *Advances in Structural Engineering*, vol. 23, no. 5, pp. 954–968, 2020.

[19] Q. Wang, Z. Li, A. Garg, B. Hazra, and Z.-N. Xie, "Effects of tuned mass damper on correlation of wind-induced responses and combination coefficients of equivalent static wind loads of high-rise buildings," *The Structural Design of Tall and Special Buildings*, vol. 28, no. 6, p. e1597, 2019.

[20] A. Giaralis and F. Petrini, "Wind-induced vibration mitigation in tall buildings using the tuned mass-damper-inerter," *Journal of Structural Engineering*, vol. 143, no. 9, Article ID 04017127, 2017.

[21] S. Elias and V. Matsagar, "Wind response control of tall buildings with a tuned mass damper," *Journal of Building Engineering*, vol. 15, pp. 51–60, 2018.

[22] Q. Wang, S. Yu, C. Ku, and A. Garg, "Combination coefficient of ESWLs of a high-rise building with an elliptical cross-section," *Wind and Structures*, vol. 31, no. 6, p. 523, 2020.

[23] A. M. Aly and S. Abburu, "On the design of high-rise buildings for multihazard: fundamental differences between wind and earthquake demand," *Shock and Vibration*, vol. 2015, Article ID 148681, 22 pages, 2015.

[24] A. Vulcano, "Comparative study of the earthquake and wind dynamic responses of base-isolated buildings," *Journal of Wind Engineering and Industrial Aerodynamics*, vol. 74–76, pp. 751–764, 1998.

[25] X.-J. Hong and M. Gu, "Probability model and solution on earthquake effects combination in along wind resistant design of tall-flexible buildings," *Applied Mathematics and Mechanics*, vol. 27, no. 5, pp. 627–636, 2006.

[26] D. Duthinh and E. Simiu, "Safety of structures in strong winds and earthquakes: multihazard considerations," *Journal of Structural Engineering*, vol. 136, no. 3, pp. 330–333, 2010.

[27] H. Mahmoud and G. Cheng, "Framework for lifecycle cost assessment of steel buildings under seismic and wind hazards," *Journal of Structural Engineering*, vol. 143, no. 3, Article ID 04016186, 2017.

[28] X.-W. Zheng, H.-N. Li, Y.-B. Yang, G. Li, L.-S. Huo, and Y. Liu, "Damage risk assessment of a high-rise building against multihazard of earthquake and strong wind with recorded data," *Engineering Structures*, vol. 200, Article ID 109697, 2019.

[29] W. Jing, H. Feng, and X. Cheng, "Dynamic responses of liquid storage tanks caused by wind and earthquake in special environment," *Applied Sciences*, vol. 9, no. 11, p. 2376, 2019.

[30] Y. Xu, T. Guo, P. Yan, and A. Li, "Effect of semiactive control on wind and seismic responses of high-rise building supported on triple friction pendulums," *Journal of Performance of Constructed Facilities*, vol. 34, no. 3, Article ID 04020035, 2020.

[31] T. Roy and V. Matsagar, "Probabilistic assessment of steel buildings installed with passive control devices under multihazard scenario of earthquake and wind," *Structural Safety*, vol. 85, Article ID 101955, 2020.

[32] L.-Y. Lu, T.-K. Lin, R.-J. Jheng, and H.-H. Wu, "Theoretical and experimental investigation of position-controlled semiactive friction damper for seismic structures," *Journal of Sound and Vibration*, vol. 412, pp. 184–206, 2018.

[33] Z. Zhang, K. Bi, H. Hao, P. Sheng, L. Feng, and D. Xiao, "Development of a novel deformation-amplified shape memory alloy-friction damper for mitigating seismic responses of RC frame buildings," *Engineering Structures*, vol. 216, Article ID 110751, 2020.

[34] D. De Domenico, N. Impollonia, and G. Ricciardi, "Seismic retrofitting of confined masonry-RC buildings: the case study of the university hall of residence in Messina, Italy," *International Journal*, vol. 36, no. 1, pp. 54–85, 2019.

[35] A. Di Matteo, A. Pirrotta, and S. Tumminelli, "Combining TMD and TLCD: analytical and experimental studies," *Journal of Wind Engineering and Industrial Aerodynamics*, vol. 167, pp. 101–113, 2017.

[36] E. Aydin, "Optimal damper placement based on base moment in steel building frames," *Journal of Constructional Steel Research*, vol. 79, pp. 216–225, 2012.

[37] E. Aydin, "A simple damper optimization algorithm for both target added damping ratio and interstorey drift ratio," *Earthquakes and Structures*, vol. 5, no. 1, pp. 83–109, 2013.

[38] D. De Domenico and G. Ricciardi, "Earthquake protection of structures with nonlinear viscous dampers optimized through an energy-based stochastic approach," *Engineering Structures*, vol. 179, pp. 523–539, 2019.

[39] E. Tubaldi, M. Barbato, and A. Dall'Asta, "Performance-based seismic risk assessment for buildings equipped with linear and nonlinear viscous dampers," *Engineering Structures*, vol. 78, pp. 90–99, 2014.

[40] Q. Wang, N. D. Tiwari, H. Qiao, and Q. Wang, "Inerter-based tuned liquid column damper for seismic vibration control of a single-degree-of-freedom structure," *International Journal of Mechanical Sciences*, vol. 184, Article ID 105840, 2020.

[41] D. De Domenico and G. Ricciardi, "Improving the dynamic performance of base-isolated structures via tuned mass damper and inerter devices: a comparative study," *Structural Control and Health Monitoring*, vol. 25, no. 10, Article ID e2234, 2018.

[42] L. Marian and A. Giaralis, "Optimal design of a novel tuned mass-damper-inerter (TMDI) passive vibration control configuration for stochastically support-excited structural systems," *Probabilistic Engineering Mechanics*, vol. 38, pp. 156–164, 2014.

[43] D. De Domenico, H. Qiao, Q. Wang, Z. Zhu, and G. Carlo Marano, "Optimal design and seismic performance of Multi-Tuned Mass Damper Inerter (MTMDI) applied to adjacent high-rise buildings," *The Structural Design of Tall and Special Buildings*, vol. 29, p. e1781, 2020.

[44] Z. Zhu, W. Lei, Q. Wang, N. Tiwari, and B. Hazra, "Study on wind-induced vibration control of linked high-rise buildings by using TMDI," *Journal of Wind Engineering and Industrial Aerodynamics*, vol. 205, Article ID 104306, 2020.

[45] GB50009-2012, *Load Code for the Design of Building Structures*, China Architecture & Building Press, Beijing, China, 2012.

[46] A. T. Council and U. S. F. E. M. Agency, *Quantification of Building Seismic Performance Factors*, US Department of Homeland Security, Washington, D. C., USA, 2009.

[47] A. Tributsch and C. Adam, "Evaluation and analytical approximation of Tuned Mass Damper performance in an earthquake environment," *Smart Structures and Systems*, vol. 10, no. 2, pp. 155–179, 2012.

[48] Q. Wang, H. Qiao, D. De Domenico, Z. Zhu, and Y. Tang, "Seismic response control of adjacent high-rise buildings linked by the tuned liquid column damper-inerter (TLCDI)," *Engineering Structures*, vol. 223, Article ID 111169, 2020.

[49] Q. Wang, H. Qiao, D. De Domenico, Z. Zhu, and Z.-N. Xie, "Wind-induced response control of high-rise buildings using inerter-based vibration absorbers," *Applied Sciences*, vol. 9, no. 23, p. 5045, 2019.

[50] J. Dai, Z.-D. Xu, and P.-P. Gai, "Tuned mass-damper-inerter control of wind-induced vibration of flexible structures based on inerter location," *Engineering Structures*, vol. 199, Article ID 109585, 2019.